34th Annual International Conference of the IEEE EMBS
San Diego, California USA, 28 August - 1 September, 2012

Quantification of uncertainties in brain tissue conductivity in a heterogeneous model of deep brain stimulation using a non-intrusive projection approach

Christian Schmidt*, Ursula van Rienen

Abstract— **The aim of this study was to examine the effects of uncertainty of the conductivity values on the resulting field distribution in a heterogeneous finite element model of deep brain stimulation (DBS). A non-intrusive projection method was used by expanding the input random variables and the resulting potential on a multidimensional basis called the Polynomial Chaos (PC). The finite element model incorporates an accurate model of a DBS electrode used in clinical treatment extended by an encapsulation layer around the electrode body. Areas of grey matter, white matter and cerebrospinal fluid were derived from averaged magnetic resonance imaging (MRI). The uncertainties of the conductivity values of these tissue types were modelled as uniform random variables using data from literature to obtain their upper and lower boundaries.**

I. INTRODUCTION

Deep brain stimulation (DBS) is a neurosurgical method to treat symptoms of motor skill disorders such as Parkinson's disease (PD), essential tremor and dystonia by implanting a stimulation electrode in a group of nuclei situated at the base of the forebrain, the basal ganglia [1]. Although the method has become a common procedure in these clinical fields [2], the fundamental mechanisms of DBS remain uncertain [3]. Starting in the last decade many models for predicting the effects of DBS were developed and more insights into the spatial extent of activation [4], the required model complexity [5] and electrode geometry were gained [6]. These models and their contribution to the understanding of the mechanisms of DBS help to develop clinical software, which could support the planning and performance of the complex stereotactic surgery as well as the prediction of longterm effects of DBS. The practical usage of such software depends on the complexity and uncertainty of the input parameters which directly influences the field distribution in the proximity of the electrode and therefore the resulting neuronal response, i.e. the activated brain regions. The uncertainty of the electrical properties of brain tissue is dependent on the experimental measurement of these properties and can vary up to a factor of 3 in literature [7].

To evaluate the influence of uncertainties in the input data of a model, popular methods based on a nonsampling approach, including perturbation methods, and those based on a sampling approach, such as Monte Carlo sampling (MCS), are commonly used. However, perturbation methods are only applicable if the magnitude of the uncertainties in the inputs and outputs are below $10\,\%$ [8]. MCS is not restricted to this limitation, but typically a large number of deterministic computations of the model is needed, since the asymptotical convergence of the statistics is $1/\sqrt{N}$, where N is the number of deterministic computations. This need for large number of executions makes MCS not applicable for 3D finite element models of DBS with up to several millions of unknowns. In contrast, the method of the polynomial chaos (PC) expresses the stochastic solutions as orthogonal polynomials of the random inputs and exploits their orthogonal nature to achieve a better convergence [8]. The method can be implemented using either an intrusive approach, in which the stochastic expansion is incorporated into the deterministic formulation, or a non-intrusive approach, in which the original determinstic formluation is maintained and used to compute the coefficients of the output expansion for given expansions of the input variables.

In this study a non-intrusive projection approach is used by expanding the random input and output on a multidimensional basis, the polynomial chaos (PC). The coefficients of the output expansion are computed by numerical evaluation of a multidimensional integral by using Gauss quadrature. In this case, the number of deterministic computations depends only on the tensor product of the used Gauss points d resulting in d^M evaluations of the finite element, where M is the number on independent random input variables.

II. METHODS

A. Polynomial chaos

The random inputs and the stochastic solutions are expressed on a truncated orthogonal basis formed by multidimensional Hermite polynomials $\psi(\boldsymbol{\xi})$ with the Gaussian random vector $\boldsymbol{\xi} = (\xi_1, \ldots, \xi_M)$ and its probality density function $f_{\boldsymbol{\xi}}$ called the polynomial chaos (PC) [9]. The random conductivity $\sigma^{(j)}$ of a certain tissue type j can then be approximated by a truncated series of multidimensional Hermite polynomials, where P_{in} is the order of the multidimensional input expansion:

$$\sigma^{(j)} \approx \sum_{i=0}^{P_{in}} \sigma_i^{(j)} \psi_i(\boldsymbol{\xi}) \quad , j = 1, \ldots, M \; . \tag{1}$$

The work was funded by the DFG (German Science Foundation) Research Training Group 1505/1 "welisa".

Asterisk indicates corresponding author.

*C. Schmidt is with the Institute of General Electrical Engineering, University of Rostock, 18057 Rostock, Germany (e-mail: christian.schmidt6@uni-rostock.de)

U. van Rienen is with the Institute of General Electrical Engineering, University of Rostock, 18057 Rostock, Germany

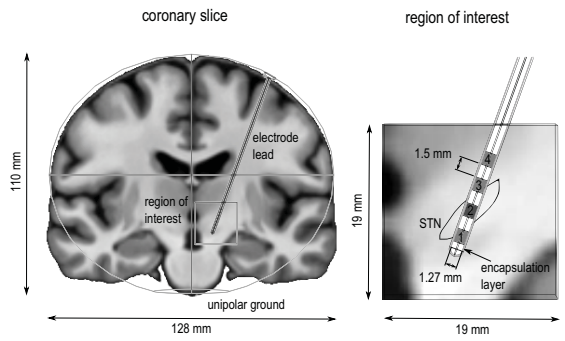

Fig. 1. Coronary slice of the model geometry consisting of a homogeneous idealized brain and a heterogeneous region of interest. The electrode tip surrounded by an encapsulation layer is located at the stimulation centre. T1 MRI data of the SRI24 multi-channel brain atlas is shown in the background. The STN is illustrated in the region of interest according to the registration with the brain atlas [10]. The four electrode contacts and the driven electrode contact 2 are highlighted in gray and dark gray, respectively.

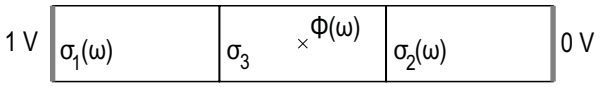

Fig. 2. Model of a 3-compartment resistor used for validation. The conductivities $\sigma_1(\omega) \in \mathcal{U}(2,4)\,\mathrm{S\,m^{-1}}$ and $\sigma_2(\omega) \in \mathcal{U}(5,9)\,\mathrm{S\,m^{-1}}$ are independent, uniformly distributed random variables, while $\sigma_3 = 10\,\mathrm{S\,m^{-1}}$ is deterministic. The random potential $\phi(\omega)$ is evaluated at the centre of the model indicated by the cross.

TABLE I

LOWER AND UPPER BOUNDARIES OF THE UNIFORMLY DISTRIBUTED RANDOM TISSUE CONDUCTIVITIES. * [7], † [14].

Brain tissue	**Min** $\left[\mathrm{S\,m^{-1}}\right]$	**Max** $\left[\mathrm{S\,m^{-1}}\right]$
White matter	0.06^{*}	$0.14^{\dagger}$
Grey matter	0.09^{*}	$0.33^{\dagger}$
Cerebrospinal fluid	$1.54^{\dagger}$	2.00^{*}

Likewise, the random output, e.g. the electrical potential at a certain node $\phi(\boldsymbol{x})$, can be expanded on the same basis, where P_{out} is the order of the multidimensional output expansion:

$$\phi(\boldsymbol{x}) \approx \sum_{k=0}^{P_{out}} \phi_k(\boldsymbol{x})\psi_k(\boldsymbol{\xi}) \ . \tag{2}$$

By computing the expectation $E[\phi(\boldsymbol{x})\psi_k(\boldsymbol{\xi})]$ and exploiting the orthogonal nature of the PC, the output coefficients $\phi_k(\boldsymbol{x})$ can be determined by the following equation:

$$\phi_k(\boldsymbol{x}) = \frac{E[\phi(\boldsymbol{x})\psi_k(\boldsymbol{\xi})]}{E[\psi_k(\boldsymbol{\xi})^2]} \ . \tag{3}$$

The denominator can be evaluated analytically while the nominator needs further consideration. In the monodimensional case, Gauss-Hermite quadrature with d Gauss points $\boldsymbol{t} = (t_1, \ldots, t_d)$ and Gauss weights $w = (w_1, \ldots, w_d)$ is used to evaluate numerically the integral by computing the deterministic solutions $\phi(\boldsymbol{x}, \sigma(\boldsymbol{t}))$. In the multidimensional case with M random inputs, the tensor product of the d Gauss points in M dimensions has to be computed, resulting in a sequence of d^M vectors $\boldsymbol{t}^{(l)} = (t_1^{(l)}, \ldots, t_M^{(l)})$ of Gauss points and weights $w^{(l)} = w_1^{(l)} \ldots w_M^{(l)}$. The multidimensional integral can then be evaluated numerically by the following equation:

$$E[\phi(\boldsymbol{x})\psi_k(\boldsymbol{\xi})] \approx \sum_{l=1}^{d^M} w^{(l)}\phi(\boldsymbol{x}, \sigma(\boldsymbol{t}^{(l)}))\psi_k(\boldsymbol{t}^{(l)}) \ . \tag{4}$$

To assess the convergence, the method was repeated for different numbers of Gauss points d while the monodimensional expansion orders were set to $p_{in} = 19$ and $p_{out} = 9$. The computation of the random input and output expansions were carried out using MATLAB (R2011b, Mathworks).

B. Model geometry

The human brain was modelled by an ellipsoid with the semi axis $64\,\mathrm{mm}$ transversal, $81\,\mathrm{mm}$ longitudinal and $55\,\mathrm{mm}$ sagittal derived from the SRI24 multi-channel brain atlas which comprises 3 T MRI images and tissue segmentations with a resolution of $1\,\mathrm{mm}^3$ of 24 volunteers spanning from 19 to 84 years old [11]. The stimulation centre is located within the STN, the position of which was determined using a brain atlas and comparing axial, coronal and sagittal slices of the T1-weighted MRI data with the location of the STN in the atlas images [10]. A model of the cylindrical stimulating electrode (Medtronic Mo. 3387, Medtronic Inc.) surrounded by an encapsulation layer with a thickness of $0.2\,\mathrm{mm}$ was incorporated into the model. The spherical angles of the electrode lead, derived from postsurgical CT scans, were set to an azimuthal angle of $7\,^\circ$ and polar angle of $20\,^\circ$. A heterogeneous region of interest (ROI) with an edge length of $19\,\mathrm{mm}$ was implemented around the electrode tip using the segmented MRI data [11]. The ground was set to a plane circle with a radius of $22\,\mathrm{mm}$ at the bottom of the model.

C. Conductivity

The conductivity of grey matter, white matter and cerebrospinal fluid are subject to uncertainty and differ in the literature [7], [12], [13]. Since the random distribution of these conductivities is not known, they are assumed here to be uniformly distributed to maximize their variance. The values for the uniform random variables were taken from [7] at $130\,\mathrm{Hz}$, which is a fundamental stimulation frequency in DBS, and [14] (see table I). The conductivity of the encapsulation layer was set to $0.135\,\mathrm{S\,m^{-1}}$ to match long term conditions of deep brain stimulation [15].

D. Finite element computation

A quasi-static approximation of the time-harmonic Maxwell's equations was used to compute the field distribution inside the brain model [16]. Since the field distribution within the ROI is of particular interest, the spatial representation of the electrode body was subtracted from the model. Boundary conditions representing perfect conductors and insulators were applied to the active electrode contact ($1\,\mathrm{V}$) as well as ground ($0\,\mathrm{V}$) and the electrode body as well as the exterior boundary of the model, respectively. The inactive electrode contacts were set to a floating potential,

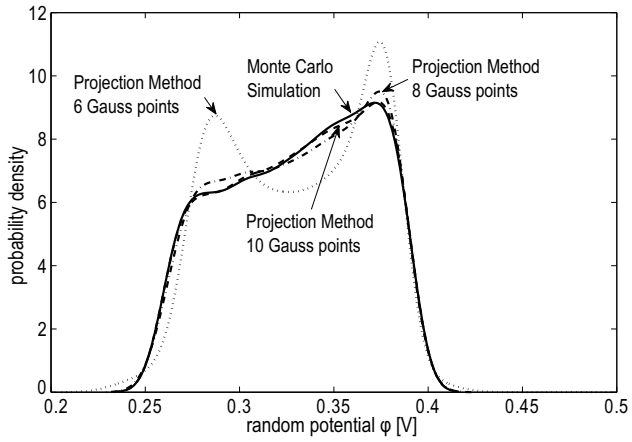

Fig. 3. Probability densities of the evaluated potential ϕ in the validation model. MCS with 7500 samples and the non-intrusive projection methods for 6, 8 and 10 Gauss points are shown.

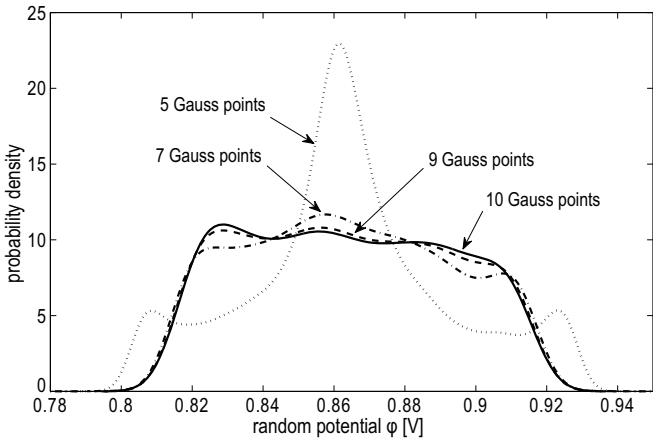

Fig. 4. Probability densities of the potential ϕ 1 mm from the active electrode contact for $10,000$ multivariate Gaussian samples. Computations were carried out for different numbers of Gauss points.

i.e. no net current flow crosses their surface. The finite element software COMSOL Multiphysics (ver 4.2, Comsol AG) was used to perform the deterministic computations. Iteration was stopped when the 2-norm of the residual was below $1 \cdot 10^{-6}$. The mesh at the electrode contact surfaces was manually refined until the alteration of the integral of the current density over the surface area was below $1\,\%$ resulting in a maximum element length of $0.2\,\mathrm{mm}$. The maximum element length within the ROI was set to $0.5\,\mathrm{mm}$ to avoid disconformities by mapping the tissue information of the hexahedral MRI mesh on the tetrahedral finite element mesh. The resulting model consisted out of 1.4 million mesh elements.

III. VALIDATION

Validation of the non-intrusive projection method was performed in a 2D quasi-static model of a 3-compartment resistor with voltages of $1\,\mathrm{V}$ and $0\,\mathrm{V}$ applied to its left and right boundaries. The conductivities of the regions were modelled using two independent, uniformly distributed random variables, $\sigma_1(\omega) \in \mathcal{U}(2,4)\,\mathrm{S\,m^{-1}}$ and $\sigma_2(\omega) \in \mathcal{U}(5,9)\,\mathrm{S\,m^{-1}}$, and one deterministic conductivity value $\sigma_3 = 10\,\mathrm{S\,m^{-1}}$ (see Fig. 2). The mesh consisted out of 228 triangular elements resulting in 517 degrees of freedom. The input and output expansions were truncated at $p_{in} = 19$ and $p_{out} = 9$, respectively. MCS for 7500 samples, resulting in the same amount of deterministic finite element executions, were carried out for the same model.

A good agreement of the results of the non-intrusive projection method with MCS could be obtained by using 10 Gauss points for which only 100 deterministic executions were necessary (see Fig. 3). The deviation of the variance of the probability density for 10 Gauss points with respect to MCS was below $5 \cdot 10^{-8}$.

IV. RESULTS

To compute the output probability density of the potential distribution around the electrode tip, multiple executions of the non-intrusive projection algorithm for different numbers of Gauss points were conducted. Using 10 Gauss points showed a good convergence of the output probability density, which approximately resembles a uniform distribution with the boundaries $\phi \approx \mathcal{U}(0.825, 0.905)\,\mathrm{V}$ (see Fig. 4). Dividing the range of the boundaries by the mean of the potential $\bar{\phi} = 0.865\,\mathrm{V}$ results in an $9.3\,\%$ uncertainty of the output potential in the proximity of the active electrode contact. To investigate the influence of the input uncertainties in the region of interest, the ouput probability density in a coronary intersection of the ROI was computed for each node on a grid with a spacing of $0.5\,\mathrm{mm}$ resulting in 1512 node points. While the mean potential in each node could be directly taken from its random expansion coefficients, the standard deviation for every node was computed using 100 multivariate Gaussian samples. Fig. 5 shows the potential isolines for $0.15\,\mathrm{V}$ and $0.25\,\mathrm{V}$ of the mean potential as well as its standard deviation. The uncertainty of the potential increases in regions which are further away from the active electrode contact, where as the potential diminuishes with increasing distance from the active electrode.

V. DISCUSSION

The uncertainty of the potential in the proximity of the active electrode contact was determined to be approximately $9.3\,\%$. This uncertainty is substantially smaller than the input uncertainties, namely $114\,\%$, $80\,\%$ and $26\,\%$ for grey matter, white matter and cerebrospinal fluid, respectively. This difference in the input and output uncertainties results from the smoothing of the potential by the Laplace equation used to compute the quasistatic solution. The potential distribution in this model is restricted to values in a limit of $0\,\mathrm{V}$ to $1\,\mathrm{V}$ predefined by the Dirichlet boundary conditions used to impose the potentials at the active electrode contact as well as the ground.

Besides the input uncertainties, the field distribution of DBS is influenced by other factors such as the frequency dependence and anisotropy of the electrical properties of the brain tissue. Deviation between frequency-fixed

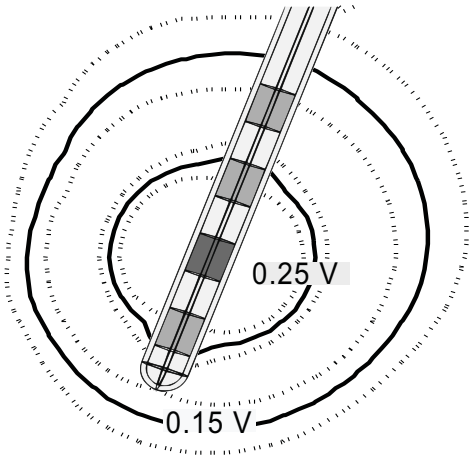

Fig. 5. Coronary slice of the mean and standard deviation of the potential distribution in the ROI. Mean potential isolines and their standard deviation are shown for $0.25\,\mathrm{V}$ and $0.15\,\mathrm{V}$. T1-weighted MRI data used to incorporate heterogeneous tissue properties in the ROI is shown in the background.

and frequency dependent quasi-static solutions for voltage-controlled stimulations were reported to be approximately $21\,\%$ [17] and $4\,\%$ between anistropic and isotropic brain models considering the neuronal activation in the STN [18]. In addition, tissue anisotropy was reported to influence the extent and shape of the potential distribution of DBS [4]. The resulting output uncertainty is strongly dependent on the uncertainties in the input data. The results of this study would therefore suggest to consider input uncertainties in models of DBS if their magnitudes are similar to those considered here.

In this study, the non-intrusive projection method was applied to the field of DBS by investigating the influence of input uncertainties of the brain tissue conductivity. Further insight could be gained by supplementary investigating uncertainties of the relative permittivity of brain tissue. However, this would require modelling of 6 random inputs resulting in exponentially increasing deterministic executions according to the curse of dimensionality. A solution to this limitation would be the use of sparse grids instead of tensor grids [9]. In addition, other sets of orthogonal polynomials such as Legendre and Laguerre polynomials could improve the convergence of the method for certain random distributions [8]. In these cases, smaller orders of expansion for the input and output could be sufficient. The presented results are not only restricted to the electric potential, but could also be used to examine the influence of uncertainties on the neuronal response in the target area.

VI. CONCLUSION

A non-intrusive projection method was used to examine the influence of uncertainties in the tissue conductivities on the field distribution for voltage-controlled stimulation in a heterogeneous model of DBS. Input uncertainties were shown to substantially influence the output potential, which suggests the importance to consider them in models of DBS.

ACKNOWLEDGMENT

The authors would like to thank Roman Gaignaire for his advice on the non-intrusive projection method. The authors would also like to thank Jan-Uwe Müller and Marc Matthes from the Department of Neurosurgery at the University Medicine Greifswald for their medical advice.

REFERENCES

[1] A. L. Benabid, "Deep brain stimulation for parkinson's disease," *Curr Opin Neurobiol*, vol. 13, pp. 696–706, 2003.
[2] E. Y. Uc and K. A. Follet, "Deep brain stimulation in movement disorders," *Semin Neurol*, vol. 27, pp. 170–182, 2007.
[3] M. C. Rodriguez-Oroz, M. Rodriguez, J. Guridi, K. Mewes, V. Chockkman, J. L. Vitek, M. R. DeLong, and J. A. Obeso, "The subthalamic nucleus in parkinson's disease: Somatotopic organization and physiological characteristics," *Brain*, vol. 124, pp. 1777–1790, 2001.
[4] C. R. Butson, S. E. Cooper, J. M. Henderson, and C. C. McIntyre, "Predicting the effects of deep brain stimulation with diffusion tensor based electric field models," *MICCAI*, pp. 429–437, 2006.
[5] A. Chaturvedi, C. R. Butson, S. F. Lempka, S. E. Cooper, and C. C. McIntyre, "Patient-specific models of deep brain stimulation: Influence of field model complexity on neural activation predictions," *Brain Stimul*, vol. 3, pp. 65–77, 2010.
[6] M. Liberti, F. Apollonio, A. Paffi, M. Parazzini, F. Maggio, T. Novellino, P. Ravazzani, and G. D'Inzeo, "Fundamental electrical quantities in deep brain stimulation: Influence of domain dimensions and boundary conditions," *P Ann Int IEEE EMBS*, pp. 6668–6671, 2007.
[7] S. Gabriel, R. W. Lau, and C. Gabriel, "The dielectric properties of biological tissues: III Parametric models for the dielectric spectrum of tissues," *Phys Med Biol*, vol. 41, pp. 2271–2293, 1996.
[8] D. Xiu, *Numerical Methods for Stochastic Computations: A Spectral Method Approach*. Princeton University Press, 2010.
[9] B. Sudret, M. Berveiller, and M. Lemaire, "A stochastic finite element procedure for moment and reliability analysis," *Eur J Comp Mech*, vol. 15, pp. 825–866, 2006.
[10] H. J. Kretschmann and W. Weinrich, *Klinische Neuroanatomie und kranielle Bilddiagnostik*. Stuttgart: Georg Thieme Verlag, 1991.
[11] T. Rohlfing, N. M. Zahr, E. V. Sullivan, and A. Pfefferbaum, "The SRI24 multi-channel brain atlas," *Proc Soc Photo Opt Instrum Eng*, vol. 6914, p. 691409, 2008.
[12] L. Geddes and L. Baker, "The specific resistance of biological material. A compendium of data for the biomedical engineer and physiologist," *Med Biol Eng*, vol. 5, pp. 271–293, 1967.
[13] S. Baumann, D. Wozny, S. Kelly, and F. C. Meno, "The electrical conductivity of human cerebrospinal fluid at body temperature," *IEEE Trans Biomed Eng*, vol. 44, pp. 220–223, 1997.
[14] M. Rullmann, A. Anwander, M. Dannhauer, S. K. Warfield, F. H. Duffy, and C. H. Wolters, "EEG source analysis of epileptiform activity using a 1 mm anisotropic hexahedra finite element head model," *NeuroImage*, vol. 44, pp. 399–410, 2009.
[15] N. Yousif and X. Liu, "Investigating the depth electrode-brain interface in deep brain stimulation using finite element models with graded compexity in structure and solution," *J Neurosci Meth*, vol. 184, pp. 142–151, 2009.
[16] C. A. Bossetti, M. J. Birdno, and W. M. Grill, "Analysis of the quasi-static approximation for calculating potentials generated by neural stimulation," *J Neural Eng*, vol. 5, pp. 44–53, 2008.
[17] P. F. Grant and M. M. Lowery, "Effect of dispersive conductivity and permittivity in volume conductor models of deep brain stimulation," *IEEE T Bio-med Eng*, vol. 57, pp. 2386–2393, 2010.
[18] S. N. Sotiropoulos and P. N. Steinmetz, "Assessing the direct effects of deep brain stimulation using embedded axon models," *J Neural Eng*, vol. 4, pp. 107–119, 2007.